# Scattering dark states in multi-resonant concentric plasmonic nanorings

Rasoul Alaee,[*,†,‡,⊥] Dennis Lehr,[¶,⊥] Robert Filter,[‡] Falk Lederer,[‡] Ernst-Bernhard Kley,[¶] Carsten Rockstuhl,[†,§] and Andreas Tünnermann[¶,‖]

*Institute of Theoretical Solid State Physics, Karlsruhe Institute of Technology, Wolfgang-Gaede-Str. 1, 76128 Karlsruhe, Germany, Institute of Condensed Matter Theory and Solid State Optics, Abbe Center of Photonics, Friedrich-Schiller-University Jena, Max-Wien-Platz 1, 07743 Jena, Germany, Institute of Applied Physics, Abbe Center of Photonics, Friedrich-Schiller-University Jena, Max-Wien-Platz 1, 07743 Jena, Germany, Institute of Nanotechnology, Karlsruhe Institute of Technology, P.O. Box 3640, 76021 Karlsruhe, Germany, and Fraunhofer Institute for Applied Optics and Precision Engineering IOF, Albert-Einstein-Str. 7, 07745 Jena, Germany*

E-mail: rasoul.khanghah@kit.edu

**Abstract**

[*]To whom correspondence should be addressed

[†]Institute of Theoretical Solid State Physics, Karlsruhe Institute of Technology, Wolfgang-Gaede-Str. 1, 76128 Karlsruhe, Germany

[‡]Institute of Condensed Matter Theory and Solid State Optics, Abbe Center of Photonics, Friedrich-Schiller-University Jena, Max-Wien-Platz 1, 07743 Jena, Germany

[¶]Institute of Applied Physics, Abbe Center of Photonics, Friedrich-Schiller-University Jena, Max-Wien-Platz 1, 07743 Jena, Germany

[§]Institute of Nanotechnology, Karlsruhe Institute of Technology, P.O. Box 3640, 76021 Karlsruhe, Germany

[‖]Fraunhofer Institute for Applied Optics and Precision Engineering IOF, Albert-Einstein-Str. 7, 07745 Jena, Germany

[⊥]These authors contributed equally to this work.

Plasmonic nanoantennas can feature a sophisticated spectral response that may be the springboard for a plethora of applications. Particularly, spectrally sharp Fano resonances have been at the focus of interest due to their promising applications in sensing. Usually, the observation of Fano resonances requires nanostructures that exhibit multiple plasmonic resonances such as higher order multipole moments. We show that similar spectral features can be observed with nanoantennas sustaining solely electric dipolar resonances. The considered nanoantennas consist of multiple concentric gold nanorings separated by thin dielectric spacers. These nanoantennas host multiple resonances with disparate line widths in the visible and near-infrared. We theoretically and experimentally show that the interference of these resonances causes Fano features and scattering dark states. The electric dipolar character permits to use a simplified dense-array theory to predict the response of arrays of such nanoantennas from the electric polarizability of the individual constituents. This paves the way for a simplified design of plasmonic meta-surfaces.

## Keywords

scattering dark states, plasmonic nanorings, fano resonances, dense array theory

Multi-resonant plasmonic nanoantennas offer possibilities for broadband sensor devices,[1–6] efficient solar cell upconverters,[7] coherent control,[8] enhanced nonlinear interactions,[9–12] and ultra-bright multiband single-photon sources working at optical and telecom frequencies.[13] From an application perspective, it is of utmost importance a) to scale the fabrication process from individual nanoantennas to large arrays,[14,15] b) to design plasmonic nanoantennas exploiting multi-resonant behavior that can be experimentally realized, and c) to have a relatively simple theoretical framework at hand to describe the optical properties of arrays in terms of the properties of the individual nanoantenna. In this contribution, we show how all aforementioned requirements can be achieved.

We consider plasmonic nanoantennas that consist of multiple concentrically aligned gold nanorings of different sizes (Fig. 1), further denoted as multi-rings. They are similar to previously discussed nanoantennas made from rings and discs.[10,16–25] These nanoantennas are known to sustain Fano resonances.[19,21] In general, Fano resonances are considered to originate from the coupling of a bright and a dark mode. In most cases the bright (continuum) mode is an electric dipole mode. The dark (discrete) mode is typically an electric quadrupole or a magnetic dipole mode (or another higher order multipole mode).[26–34] These higher order multipolar modes couple only weakly to free space radiation. This causes a narrower line width of the resonance and losses are ultimately dominated by absorption rather than by radiation. The spectral interference of bright and dark modes causes an asymmetric line-shape in the scattering signal or in the reflectance and transmittance spectra of a periodic arrangement of the nanoantennas.

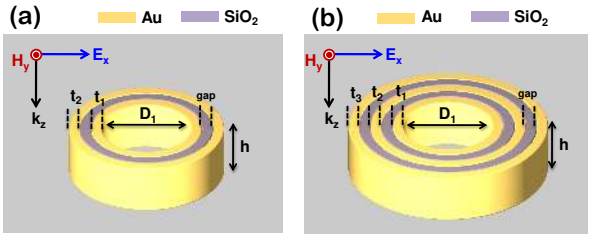


Figure 1: Schematic representation of a nanoantenna in air made of multiple concentric plasmonic nanorings: (a) two gold nanorings, (b) three gold nanorings. The dielectric spacer has a refractive index of $n = 1.46$.

Nevertheless, different multipolar resonances are not required to observe Fano features.[26,27,35–37] What is usually considered as required is a largely disparate line width.[35] This line width can be tailored at the single nanoantenna level. Indeed, it has been previously suggested that plasmonic ring structures experience lower absorption losses for thinner metallic rings or larger radii.[17–20] This renders their line width to be sufficiently narrow.

The lowest order resonance of a plasmonic ring is electric dipolar.[14,16,20,22] It is a bonding state of the hybridized surface plasmons at the inner and outer circumference.[14,16,20,22] In the following we will expose that higher order modes in multi-rings are also solely dipolar.

This offers the opportunity to have multiple narrow electric dipolar resonances across a wide frequency range which spectrally interfere and cause a Fano line-shape.

The emergence of spectrally overlapping resonances in the same scattering channel with equal angular momentum and polarization has only recently been suggested to lead to a scattering dark state.[38] For such a state, the scattering of a single nanoantenna is strongly suppressed. This phenomenon is robust against absorption, which makes the observation of scattering dark states with plasmonic structures feasible. We expect multi-rings to exhibit such states because of the fact that they feature spectrally overlapping resonances. The appearance of scattering dark states can be understood both in terms of a mutual coupling of the modes in the near-field but also as a coherent interference in the far-field.[38] For a periodic arrangement of such nanoantennas, the occurrence of scattering dark states shall translate into an asymmetric line-shape and a suppressed reflection at the frequency of the scattering dark state.

In this contribution, we theoretically and experimentally explore such phenomena with the example of a multi-ring nanoantenna. Contrary to the usual Fano schemes frequently discussed, the resonances of the multi-ring nanoantenna are entirely electric dipolar in nature. This allows to use a simple dense-array theory to predict the response of arrays of such nanoantennas from the scattering response of its individual constituents. With that, a very handy and versatile quasi-analytical theory is available that can predict the optical response of macroscopic samples. This is similar to the description of Fano features in nanohole arrays.[36,37,39] Our theory provides unique insights into the design of meta-surfaces whose optical properties can be understood not just by full-wave simulations but also by more analytically oriented theories.

## Numerical and Theoretical Results

Figure 1 shows a schematic of the studied multi-ring antenna. For all numerical simulations, the height of nanorings is $h = 75\,\mathrm{nm}$ and the diameter of the inner nanoring ($D_1$) is $100\,\mathrm{nm}$. For now, the nanoantennas are embedded in vacuum and are illuminated by an $x$-polarized plane wave propagating in the $z$-direction [Fig. 1]. The numerical calculations were performed with COMSOL.[40] The method solves Maxwell's equations in frequency space using a finite-element method. The dispersive permittivity of the gold has been taken from Ref.[41] More details on the calculation of the total scattering cross-section $C_{\mathrm{sca}}$ and $p_x$ can be found in the literature.[42] In general, the numerically calculated scattered field is projected onto the analytically known fields of elementary multipolar sources. The multipole moments of the source are unambiguously retrieved by using a suitable normalization. Finally, the retrieved multipole moments are used to calculate their contribution to the total scattering cross section.[42,43]

Before considering a periodic array of multi-rings, we numerically investigate the scattering response of individual multi-rings. The total scattering cross section versus frequency $\nu$ for multi-rings with two and three gold rings is shown in Fig. 2 (a) and (b), respectively. The scattering response of the nanoantennas is readily explained by its electric dipole moment [red dashed lines in Fig. 2 (a) and (b)]; all higher-order multipoles are negligible.

For an $x$-polarized plane wave illumination, the induced electric dipole moment of the investigated nanoantennas can be calculated as $p_{\mathrm{x}} = \varepsilon_0 \alpha_{\mathrm{ee}} E_{\mathrm{x}}$, since no cross-polarized electric dipole moments are induced. The real and imaginary parts of the electric polarizability $\alpha_{\mathrm{ee}}$ are shown in Fig. 2 (c) and (d). The electric polarization indicates the existence of two/three modes for two/three gold rings. The line width of the $1^{\mathrm{st}}$ mode is very broad compared to the higher modes. Consequently, the $1^{\mathrm{st}}$ mode can be considered as a continuum mode whereas the higher modes which exhibit a larger quality factor can be considered discrete. These higher order modes are the dipolar resonances of rings with increasing radius. The resonance positions are clearly encountered as a resonant modulation in the total scattering cross section

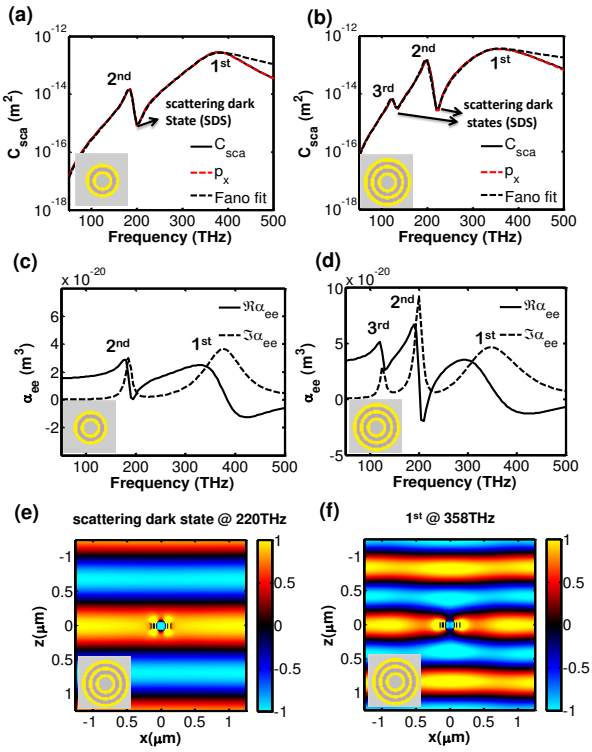


Figure 2: (a) and (b) Scattering cross section (black line) and the contribution to the scattering cross section of the electric dipole moment (red dashed line) as a function of frequency for two and three concentric nanorings, respectively. The black dashed lines show the Fano fit of the spectra. (c) and (d) The corresponding individual electric polarizabilities calculated by multipole expansion of the scattered field. (e) and (f) Field distributions ($E_{\mathrm{x}}$) for the scattering dark state (220 THz) and the 1$^{\mathrm{st}}$ mode (358 THz) of the three ring configuration. The thickness of each layer (gold/dielectric) is $t_1 = t_2 = t_3 = \mathrm{gap} = 20\,\mathrm{nm}$.

spectrum on top of the broad background caused by the 1st mode. Between the peaks, in the total scattering cross section spectrum, the scattering response is suppressed by a coherent interference of the continuum and a discrete mode [Fig. 2 (a) and (b)]. This phenomenon is known as a scattering dark state, which always appears between two scattering peaks[38] and can be due to a Fano resonance.[26] It is important to note again that the Fano resonance in the investigated multi-rings is only due to electric dipole modes, which is different from usually discussed plasmonic Fano resonances.[26] Scattering dark states exhibit a strongly suppressed scattering response in the far field [Fig. 2 (a) and (b)]. For example, the three-ring nanoantenna is hardly visible at $\nu = 220\,\mathrm{THz}$ [Fig. 2 (e)]. At this frequency, the illumination causes a field enhancement in the near-field, but the far-field remains unperturbed. In contrast, the illumination is considerably scattered at the resonance frequency (358 THz) of the 1st mode [Fig. 2 (f)].

Table 1: Fitting parameters for the spectra discussed in Fig. 2 (a)-(b) [see back dashed lines] by using Eq. (1) and Eq. (2). Note that Fig. 2 (b) has two Fano resonances (i.e. the 2nd and 3rd modes). $\nu_{1a}$ and $\nu_{2a}$ are the central frequencies of the 2nd and 3rd modes of the calculated spectra, respectively. $q_1$, $q_2$ are the corresponding asymmetric parameters.

| | $a^2\,(m^2)$ | $\nu_s\,(\mathrm{THz})$ | $W_s\,(\mathrm{THz})$ | $\nu_{1a}\,(\mathrm{THz})$ | $\nu_{2a}\,(\mathrm{THz})$ | $W_{1a}\,(\mathrm{THz})$ | $W_{2a}\,(\mathrm{THz})$ | $q_1$ | $q_2$ | $b_1$ | $b_2$ |
|---|---|---|---|---|---|---|---|---|---|---|---|
| Fig. 2 (a) | $2.7\times10^{-13}$ | 365 | 60 | 185 | - | 8 | - | −1.9 | – | 1 | - |
| Fig. 2 (b) | $2.95\times10^{-13}$ | 325 | 70 | 195 | 123 | 8 | 8 | −3 | −0.75 | 1 | 1.5 |

In order to quantitatively discuss the Fano features of the calculated spectra $C_{\mathrm{sca}}\,(\nu)$ [see Fig. 2 (a) and (b)], we used a well-known fitting function. The fitting function is a product of the Fano line-shape spectra $C_{\mathrm{Fano}}\,(\nu)$ and the Lorentzian line-shape spectra $C_{\mathrm{Lorentz}}\,(\nu)$, i.e. $C_{\mathrm{sca}}\,(\nu) = C_{\mathrm{Fano}}\,(\nu)\,C_{\mathrm{Lorentz}}\,(\nu)$.[33,44] The Fano line-shape spectra $C_{\mathrm{Fano}}\,(\nu)$ is given by

$$C_{\mathrm{Fano}}\,(\nu) \;=\; \frac{\left(\frac{\nu^2-\nu_a^2}{2W_a\nu_a}+q\right)^2+b}{\left(\frac{\nu^2-\nu_a^2}{2W_a\nu_a}\right)^2+1}, \qquad (1)$$

where $q$ is the Fano (asymmetric) parameter, $\nu_a$ is the central frequency with spectral width $W_a$, and $b$ is the modulation damping. Moreover, the Lorentzian line-shape reads as

$$C_{\text{Lorentz}}(\nu) = \left(\frac{\nu}{\nu_s}\right)^4 \frac{a^2}{\left(\frac{\nu^2-\nu_s^2}{2W_s\nu_s}\right)^2 + 1}, \tag{2}$$

where $\nu_s$ is the central frequency with spectral width $W_s$ and $a$ is the maximum amplitude of the resonance.[44] All the fitting parameters for Fig. 2 (a) and (b) can be found in Table. 1. It can be seen that the fitted spectra [see black dashed lines in Fig. 2 (a) and (b)] are in good agreement with the simulation results. The fitting parameters confirm a large asymmetry and thus Fano features in the simulated spectra.

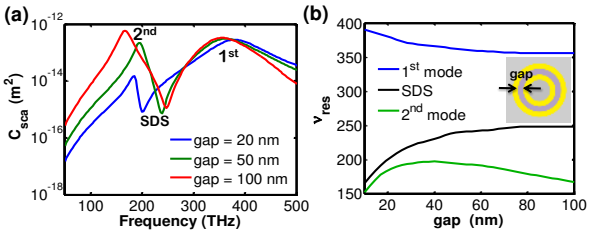


Figure 3: (a) Scattering cross sections of two concentric nanorings as a function of frequency for different dielectric spacers (gap). (b) The resonance frequency of the 1st mode and 2nd modes as well as scattering dark state (SDS) as a function of the dielectric spacer (gap). The thickness of each gold layer is $t_1 = t_2 = 20\,\text{nm}$.

In order to investigate the robustness of the observed optical features, i.e. the scattering dark state and the asymmetric Fano line-shape, we calculated the scattering cross sections of the two concentric nanorings for different dielectric spacers, i.e. gaps between the metallic rings. Figure 3 (a) depicts the scattering cross sections as a function of frequency for different dielectric spacers, i.e. gap $= 20, 50, 100\,\text{nm}$. It can be seen that the amplitude and bandwidth of the 2nd mode can be widely tuned and enhanced by increasing the gap. However, the amplitude of the 1st mode is almost fixed. This allows to tune the position of the scattering dark state over a broad range of frequency [Fig. 3 (b)]. Moreover, we also calculated the scattering cross section for various gold thicknesses.Exemple are shown for $t_2 = 20, 40, 60\,\text{nm}$ in Fig. 4 (a). It can be seen that the amplitude and resonance position of the scattering dark

state can be easily tuned by adopting this parameter as well [see Fig. 4 (b)]. Therefore, we can conclude that these features are quite robust against changes in the dimensions of the investigated nanoantenna.

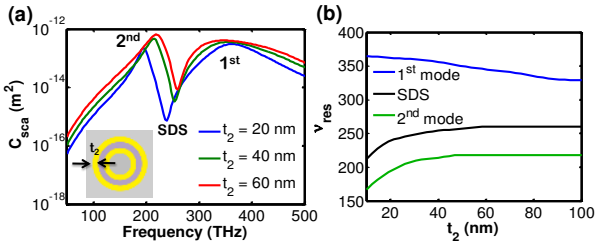


Figure 4: (a) Scattering cross sections of two concentric nanorings as a function of frequency for different gold thicknesses, i.e. $t_2 = 20, 40, 60$ nm. (b) The resonance frequency of the $1^{\text{st}}$ mode and $2^{2\text{nd}}$ modes as well as scattering dark state (SDS) as a function of gold thickness. The thickness of first ring gold layer is $t_1 = 20\,\text{nm}$, and the dielectric spacer is gap $= 50\,\text{nm}$,.

The scattering response of an isolated multi-ring at normal incidence can be solely explained by its electric polarizability $\alpha_{ee}$. In a dipole approximation, a simplified dense-array theory can be used to calculate the reflection $r$ and transmission $t$ coefficients of a periodic array of these multi-rings:[42,45,46]

$$r = \frac{i\omega}{2\Lambda^2 c_0}\frac{\alpha_{\text{ee}}}{1-\varepsilon_0\alpha_{\text{ee}}\beta_{\text{ee}}} \tag{3}$$

$$t = 1+\frac{i\omega}{2\Lambda^2 c_0}\frac{\alpha_{\text{ee}}}{1-\varepsilon_0\alpha_{\text{ee}}\beta_{\text{ee}}}\,. \tag{4}$$

Here, $\Lambda$ is the period of the array, $c_0$ is the speed of light, $\varepsilon_0$ is the vacuum permittivity, and $\omega = 2\pi\nu$ is the angular frequency. The interaction constant $\beta_{\text{ee}}$ is given by[45]

$$\beta_{\text{ee}} = i\frac{Z_0\omega}{4\Lambda^2}\left(1+\frac{1}{ikR_0}\right)e^{ikR_0}\,, \tag{5}$$

where $R_0 = \Lambda/1.438$ is the effective inter-particle distance,[47] $Z_0 = 1/\varepsilon_0 c_0$ is the free space impedance and $k = \omega/c_0$ is the vacuum wavenumber. A monochromatic field ($\propto e^{-i\omega t}$) has been assumed. Reflection and transmission spectra are sketched in Fig. 5 (c) and (d) based on Eq. (3) and Eq. (4) and compared with rigorous numerical simulations. At lower

frequencies, the numerical results are in excellent agreement with theory. A redshift of the numerical results occurs at higher frequencies, because the wavelength gets comparable to the actual size of the multi-rings and retardation effects come into play. As highlighted already, the strongly asymmetric line-shapes of the reflection and transmission spectra are due to interference of different dipole modes. It is remarkable that in a small frequency range, e.g. for the three gold ring structure between 200-220 THz, the transmission and reflection of the array changes drastically. Besides the Fano resonances, this is a direct evidence of enhanced transmission of the scattering dark states as well. Whereas the scattering dark state is clearly visible in reflection, the transmission does not reach unity because of a remaining absorption, i.e. extinction remains finite.

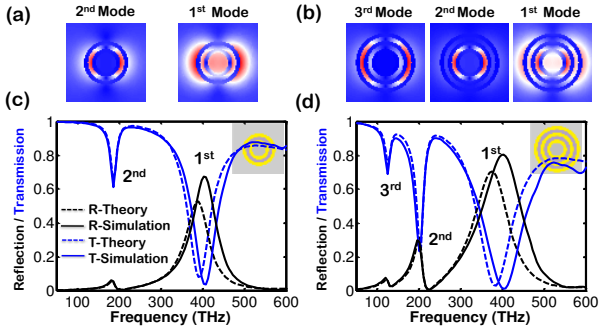


Figure 5: (a) and (b) The electric field distributions ($|\mathbf{E}|/|\mathbf{E}_{\rm inc}|$) for all modes of the two and three concentric nanorings, respectively. (c) and (d) Simulation (solid lines) and theoretical [dashed lines, based on Eq. (3) and Eq. (4)] transmission (T) and reflection (R) spectra for the array of such multi-rings with period $\Lambda = 500\,\mathrm{nm}$. The thickness of each layer (gold/dielectric) is $t_1 = t_2 = t_3 = \mathrm{gap} = 20\,\mathrm{nm}$.

The electric field distributions for all modes are shown in Fig. 5 (a) and (b). The continuum ($1^{\rm st}$) mode is dominated by the electric dipolar response of the entire nanoantenna. This mode is super-radiant and leads to the large radiation dominated line width. It provides a uniform field enhancement inside the innermost nanoring [Fig. 5 (a)]. Similar modes can also be found in a single ring nanoantennas.[14–16,18,20] The higher order modes are caused by an anti-symmetric coupling of dipolar modes of the individual rings, which effectively reduces their radiative yield. However, they do exhibit a net-dipole moment in the far-field. The higher order modes are localized inside the dielectric spacer between two gold nanorings.

Such highly concentrated gap modes might be used for coherent control,[8] to boost nonlinear effects[9,10] or to access dipole-forbidden transitions of quantum systems.[48]

## Experimental Realization and Discussion

To underline the relevance and applicability of the investigated multi-rings, we extended our existing efficient and large-scale single-ring fabrication process to multi-rings. The basic process has been explained in details in Ref.[15] Hence, we limit the following description to the basic fabrication scheme [Fig. 6 (a)]. To fabricate the inner rings, resist pillars are generated on a fused silica substrate by means of character projection electron beam lithography. In the next step, the resist pillars are homogeneously coated with gold by physical vapour deposition. To obtain a ring, the coating material is removed from horizontal surfaces by ion beam etching. The extension from single to multi-rings was realized by repeating the coating and ion beam etching step and alternating the coating material between gold and silicon dioxide. After assembly of the last concentric ring, the resist pillar in the core is removed by an oxygen plasma. Our approach allows the realization of multi-ring arrays with geometrical features and gaps below 20 nm and delivers a pattern efficiency of square decimeters in a reasonable time-span of hours.[15,49] The measurements is performed by a PerkinElmer Lambda 950 spectrophotometer with unpolarized light.

We performed numerical simulations and compared them to the measured reflection and transmission of the fabricated samples. This provides evidence for the anticipated spectral features and allows assessing the quality of the samples [Fig. 6 (d) and (e)]. Excellent agreement is observed upon considering fine details of the samples. Specifically, it was found that the involved etching processes causes redeposition of etched material at the metal-interface of the nanorings. The redeposited material originates from the vicinity of the nanorings and is likely a mixture of silicon dioxide and chromium, which was used as masking material for etching the resist pillars.

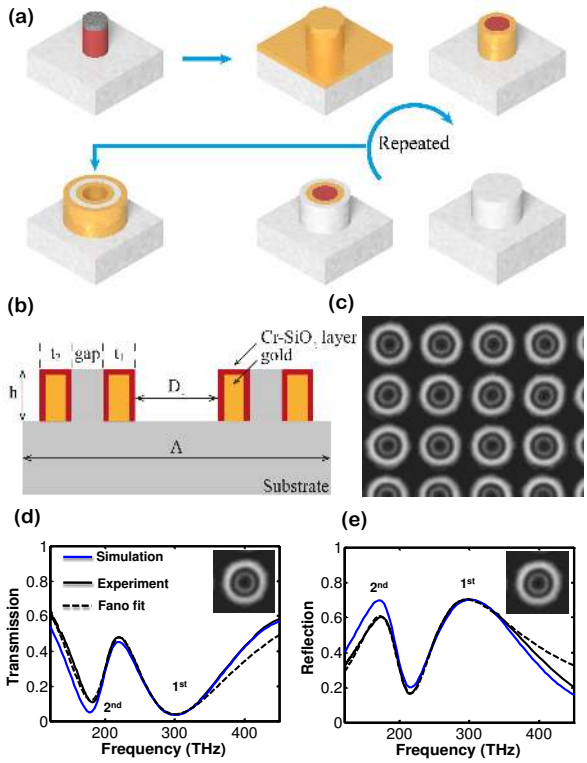


Figure 6: (a) Sketches of various steps to fabricate investigated nanorings. (b) Sketch of the simulated structure. (c) SEM image of the fabricated sample. (d) Simulated, measured, and the corresponding Fano fit of the transmission spectra for two concentric gold nanorings. (e) The same for the reflection spectra. The dimensions of the two concentric nanorings are $D_1 = 100$ nm, $t_1 = 23$ nm, gap $= 36$ nm, $t_2 = 66$ nm. The array is placed on a dielectric substrate (fused silica) with a refractive index of $n = 1.46$.

To precisely model the fabricated sample, those redepositions have to be considered in the simulations. Therefore, we used a very simplified model in complete analogy to Reference.[14] We introduced an additional homogenous layer at the metal interfaces, which were exposed to the ion beam during the etching process [Fig. 6 (c)]. The optical properties of this layer are described by an effective index derived from an effective medium theory considering a material consisting of 50 percent chromium and 50 percent silicon dioxide.[14] The geometrical parameters used in the simulation model were taken from scanning electron micrographs, i.e. $D_1 = 100$ nm, $t_1 = 23$ nm, gap $= 36$ nm, $t_2 = 66$ nm. By fitting the simulation results to the measured spectra, we determined a thickness 3 nm for the layer describing the redeposited material. Despite the simplification assumed in the model, it seems adequate to describe the experimental results.

Table 2: Fitting parameters for Fig. 6 (d) and (e) [see black dashed lines] by using Eq. 6.

| | $a^2$ | $\nu_s$ (THz) | $W_s$ (THz) | $\nu_a$ (THz) | $W_a$ (THz) | $q$ | $b$ |
|---|---|---|---|---|---|---|---|
| Fig. 6 (d) | 1.05 | 210 | 136 | 196 | 38 | −0.47 | 0.62 |
| Fig. 6 (e) | 0.98 | 216 | 110 | 194 | 38 | −0.55 | 0.23 |

In order to fit the measured reflection spectra to an analytical model and to extract the parameters that quantify the Fano features, we used a similar expression of the assumed scattering cross section [Eq. (1) and Eq. (2)]:

$$R_{\mathrm{Fit}} = \left[\frac{\left(\frac{\nu^2-\nu_a^2}{2W_a\nu_a}+q\right)^2+b}{\left(\frac{\nu^2-\nu_a^2}{2W_a\nu_a}\right)^2+1}\right]\left[\left(\frac{\nu}{\nu_s}\right)^2\frac{a^2}{\left(\frac{\nu^2-\nu_s^2}{2W_s\nu_s}\right)^2+1}\right]. \quad (6)$$

Note that the measured transmission spectra is fitted by $1 - R_{\mathrm{Fit}}$. All the fitting parameters can be found in Table. 2. These Fano parameters, i.e. $q$ and $b$ confirm that the spectra pos-

sess notable asymmetric line-shapes. However, enhanced transmission and scattering dark states are less pronounced. This is in fact related to the increased absorption of a 3 nm Cr-$SiO_2$ redeposited layer [see Fig. 6 (b)] which can be avoided, in general, by using another fabrication technique.[10] Moreover, the substrate also partially destroys these features. Nevertheless, they can be fully lifted by embedding the entire structure in a uniform medium with a refractive index corresponding to that of the substrate ($SiO_2$). Further simulations (not shown here) confirm that these two features (scattering dark state and enhanced transmission) are pronounced for an ideal structure (i.e. without Cr-$SiO_2$ redeposited layer) which is embedded in homogenous media.

# Conclusion

In conclusion, we have introduced a new type of multi-resonant plasmonic nanoantenna based on concentric nanorings that shows some remarkable optical features, i.e. Fano resonances that cause enhanced and fully suppressed scattering. Dense-array theory can be applied to the investigated concentric nanorings to predict the optical response of an associated array based on the polarizability of the isolated nanoantenna. The numerically calculated response of such arrays agrees well with the dense-array predictions and experimental data. The distinguished field concentration of the modes inside of the dielectric spacer makes concentric nanorings an interesting platform for enhanced light-matter-interactions, especially for multiresonant systems. Furthermore, the fabrication method enables a large-scale, deterministic and reproducible realization of multiresonant nanostructures with nanometric gaps.

## Acknowledgement

We thank the German Federal Ministry of Education and Research(PhoNa, 03IF2101A), the Thuringian State Government(MeMa, PE116-1) and the DFG project MetaLiquid (KL 1199/6-1, RO 3640/3-1). The authors thank Dr. Ivan Fernandez-Corbaton for his construc-

tive comments and suggestions.

## References

(1) Aydin, K.; Ferry, V. E.; Briggs, R. M.; Atwater, H. A. Broadband polarization-independent resonant light absorption using ultrathin plasmonic super absorbers. *Nat Commun* **2011**, *2*, 517.

(2) Alaee, R.; Menzel, C.; Huebner, U.; Pshenay-Severin, E.; Bin Hasan, S.; Pertsch, T.; Rockstuhl, C.; Lederer, F. Deep-Subwavelength Plasmonic Nanoresonators Exploiting Extreme Coupling. *Nano Letters* **2013**, *13*, 3482–3486, PMID: 23805879.

(3) Huebner, U.; Pshenay-Severin, E.; Alaee, R.; Menzel, C.; Ziegler, M.; Rockstuhl, C.; Lederer, F.; Pertsch, T.; Meyer, H.-G.; Popp, J. Exploiting extreme coupling to realize a metamaterial perfect absorber. *Microelectronic Engineering* **2013**, *111*, 110 – 113.

(4) Liu, N.; Mesch, M.; Weiss, T.; Hentschel, M.; Giessen, H. Infrared Perfect Absorber and Its Application As Plasmonic Sensor. *Nano Lett.* **2010**, *10*, 2342–2348.

(5) Monticone, F.; Argyropoulos, C.; Alù, A. Multilayered Plasmonic Covers for Comblike Scattering Response and Optical Tagging. *Phys. Rev. Lett.* **2013**, *110*, 113901.

(6) Monticone, F.; Argyropoulos, C.; Alu, A. Layered plasmonic cloaks to tailor the optical scattering at the nanoscale. *Sci. Rep.* **2012**, *2*, –.

(7) Atwater, H. A.; Polman, A. Plasmonics for improved photovoltaic devices. *Nat Mater* **2010**, *9*, 205–213.

(8) leveque, G.; Martin, O. Narrow-band multiresonant plasmon nanostructure for the coherent control of light: an optical analog of the xylophone. *Physical review letters* **2008**, *100*, 117402.

(9) Metzger, B.; Schumacher, T.; Hentschel, M.; Lippitz, M.; Giessen, H. Third Harmonic Mechanism in Complex Plasmonic Fano Structures. *ACS Photonics* **2014**, *1*, 471–476.

(10) Lehr, D.; Reinhold, J.; Thiele, I.; Hartung, H.; Dietrich, K.; Menzel, C.; Pertsch, T.; Kley, E.-B.; TÃijnnermann, A. Enhancing Second Harmonic Generation in Gold Nanoring Resonators Filled with Lithium Niobate. *Nano Letters* **2015**, *15*, 1025–1030, PMID: 25584636.

(11) Linden, S.; Niesler, F. B. P.; Förstner, J.; Grynko, Y.; Meier, T.; Wegener, M. Collective Effects in Second-Harmonic Generation from Split-Ring-Resonator Arrays. *Phys. Rev. Lett.* **2012**, *109*, 015502.

(12) Cai, W.; Vasudev, A. P.; Brongersma, M. L. Electrically Controlled Nonlinear Generation of Light with Plasmonics. *Science* **2011**, *333*, 1720–1723.

(13) Filter, R.; Słowik, K.; Straubel, J.; Lederer, F.; Rockstuhl, C. Nanoantennas for ultrabright single photon sources. *Opt. Lett.* **2014**, *39*, 1246–1249.

(14) Lehr, D.; Dietrich, K.; Helgert, C.; Käsebier, T.; Fuchs, H.-J.; Tünnermann, A.; Kley, E.-B. Plasmonic properties of aluminum nanorings generated by double patterning. *Opt. Lett.* **2012**, *37*, 157–159.

(15) Lehr, D.; Alaee, R.; Filter, R.; Dietrich, K.; Siefke, T.; Rockstuhl, C.; Lederer, F.; Kley, E.-B.; TÃijnnermann, A. Plasmonic nanoring fabrication tuned to pitch: Efficient, deterministic, and large scale realization of ultra-small gaps for next generation plasmonic devices. *Applied Physics Letters* **2014**, *105*, 143110.

(16) Aizpurua, J.; Hanarp, P.; Sutherland, D. S.; Käll, M.; Bryant, G. W.; Garcia de Abajo, F. J. Optical Properties of Gold Nanorings. *Phys. Rev. Lett.* **2003**, *90*, 057401.

(17) Hao, F.; Nordlander, P.; Burnett, M. T.; Maier, S. A. Enhanced tunability and linewidth

sharpening of plasmon resonances in hybridized metallic ring/disk nanocavities. *Phys. Rev. B* **2007**, *76*, 245417.

(18) Hao, F.; Larsson, E. M.; Ali, T. A.; Sutherland, D. S.; Nordlander, P. Shedding light on dark plasmons in gold nanorings. *Chemical Physics Letters* **2008**, *458*, 262–266.

(19) Hao, F.; Nordlander, P.; Sonnefraud, Y.; Dorpe, P. V.; Maier, S. A. Tunability of Subradiant Dipolar and Fano-Type Plasmon Resonances in Metallic Ring/Disk Cavities: Implications for Nanoscale Optical Sensing. *ACS Nano* **2009**, *3*, 643–652.

(20) Nordlander, P. The Ring: A Leitmotif in Plasmonics. *ACS Nano* **2009**, *3*, 488–492.

(21) Sonnefraud, Y.; Verellen, N.; Sobhani, H.; Vandenbosch, G. A.; Moshchalkov, V. V.; Van Dorpe, P.; Nordlander, P.; Maier, S. A. Experimental Realization of Subradiant, Superradiant, and Fano Resonances in Ring/Disk Plasmonic Nanocavities. *ACS Nano* **2010**, *4*, 1664–1670, PMID: 20155967.

(22) Tsai, C.-Y.; Lu, S.-P.; Lin, J.-W.; Lee, P.-T. High sensitivity plasmonic index sensor using slablike gold nanoring arrays. *Applied Physics Letters* **2011**, *98*, 153108.

(23) Near, R.; Tabor, C.; Duan, J.; Pachter, R.; El-Sayed, M. Pronounced Effects of Anisotropy on Plasmonic Properties of Nanorings Fabricated by Electron Beam Lithography. *Nano Lett.* **2012**, *12*, 2158–2164.

(24) Toma, M.; Cho, K.; Wood, J.; Corn, R. Gold Nanoring Arrays for Near Infrared Plasmonic Biosensing. *Plasmonics* **2014**, *9*, 765–772.

(25) Rakovich, A.; Albella, P.; Maier, S. A. Plasmonic Control of Radiative Properties of Semiconductor Quantum Dots Coupled to Plasmonic Ring Cavities. *ACS Nano* **0**, *0*, null, PMID: 25602764.

(26) Miroshnichenko, A. E.; Flach, S.; Kivshar, Y. S. Fano resonances in nanoscale structures. *Rev. Mod. Phys.* **2010**, *82*, 2257–2298.

(27) Luk'yanchuk, B.; Zheludev, N. I.; Maier, S. A.; Halas, N. J.; Nordlander, P.; Giessen, H.; Chong, C. T. The Fano resonance in plasmonic nanostructures and metamaterials. *Nat Mater* **2010**, *9*, 707–715.

(28) Wei, L.; Miroshnichenko, A. E.; Kivshar, Y. S. Control of light scattering by nanoparticles with optically-induced magnetic responses. *Chinese Physics B* **2014**, *23*, 047806.

(29) Singh, R.; Al-Naib, I. A. I.; Koch, M.; Zhang, W. Sharp Fano resonances in THz metamaterials. *Opt. Express* **2011**, *19*, 6312–6319.

(30) Zhao, J.; Zhang, C.; Braun, P. V.; Giessen, H. Large-Area Low-Cost Plasmonic Nanostructures in the NIR for Fano Resonant Sensing. *Advanced Materials* **2012**, *24*, OP247–OP252.

(31) Liu, W.; Miroshnichenko, A. E.; Neshev, D. N.; Kivshar, Y. S. Polarization-independent Fano resonances in arrays of core-shell nanoparticles. *Phys. Rev. B* **2012**, *86*, 081407.

(32) Ruan, Z.; Fan, S. Superscattering of Light from Subwavelength Nanostructures. *Phys. Rev. Lett.* **2010**, *105*, 013901.

(33) Gallinet, B.; Martin, O. J. F. *Ab initio* theory of Fano resonances in plasmonic nanostructures and metamaterials. *Phys. Rev. B* **2011**, *83*, 235427.

(34) Hancu, I. M.; Curto, A. G.; Castro-López, M.; Kuttge, M.; van Hulst, N. F. Multipolar interference for directed light emission. *Nano Letters* **2013**, *14*, 166–171.

(35) Fano, U. Effects of Configuration Interaction on Intensities and Phase Shifts. *Phys. Rev.* **1961**, *124*, 1866–1878.

(36) Genet, C.; van Exter, M.; Woerdman, J. Fano-type interpretation of red shifts and red tails in hole array transmission spectra. *Optics Communications* **2003**, *225*, 331 – 336.

(37) Sarrazin, M.; Vigneron, J.-P.; Vigoureux, J.-M. Role of Wood anomalies in optical properties of thin metallic films with a bidimensional array of subwavelength holes. *Phys. Rev. B* **2003**, *67*, 085415.

(38) Hsu, C. W.; DeLacy, B. G.; Johnson, S. G.; Joannopoulos, J. D.; Soljacic, M. Theoretical Criteria for Scattering Dark States in Nanostructured Particles. *Nano Letters* **2014**, *14*, 2783–2788, PMID: 24805881.

(39) Altewischer, E.; Ma, X.; van Exter, M. P.; Woerdman, J. P. Fano-type interference in the point-spread function of nanohole arrays. *Opt. Lett.* **2005**, *30*, 2436–2438.

(40) Multiphysics, C. 4.3 User's Guide. 2012.

(41) Johnson, P. B.; Christy, R. W. Optical Constants of the Noble Metals. *Phys. Rev. B* **1972**, *6*, 4370–4379.

(42) Mühlig, S.; Menzel, C.; Rockstuhl, C.; Lederer, F. Multipole analysis of meta-atoms. *Metamaterials* **2011**, *5*, 64–73.

(43) Bernal Arango, F.; Coenen, T.; Koenderink, A. F. Underpinning Hybridization Intuition for Complex Nanoantennas by Magnetoelectric Quadrupolar Polarizability Retrieval. *ACS Photonics* **2014**, *1*, 444–453.

(44) Gallinet, B.; Martin, O. J. F. Influence of Electromagnetic Interactions on the Line Shape of Plasmonic Fano Resonances. *ACS Nano* **2011**, *5*, 8999–9008, PMID: 22026329.

(45) Tretyakov, S. *Analytical modeling in applied electromagnetics*; Artech House, 2003.

(46) Alaee, R.; Albooyeh, M.; Yazdi, M.; Komjani, N.; Simovski, C.; Lederer, F.; Rockstuhl, C. Magnetoelectric coupling in nonidentical plasmonic nanoparticles: Theory and applications. *Phys. Rev. B* **2015**, *91*, 115119.

(47) Collin, R. E. *Field theory of guided waves*; McGraw-Hill, 1960.

(48) Filter, R.; Mühlig, S.; Eichelkraut, T.; Rockstuhl, C.; Lederer, F. Controlling the dynamics of quantum mechanical systems sustaining dipole-forbidden transitions via optical nanoantennas. *Phys. Rev. B* **2012**, *86*, 035404.

(49) Kley, E.-B.; Schmidt, H.; Zeitner, U.; Banasch, M.; Schnabel, B. Enhanced E-beam pattern writing for nano-optics based on character projection. 28th European Mask and Lithography Conference (EMLC 2012). 2012; pp 83520M–83520M.

# Graphical TOC Entry